Ordering transition of non-Brownian suspensions in confined steady shear flow

Kyongmin Yeo and Martin R. Maxey*
Division of Applied Mathematics, Brown University, Providence, Rhode Island 02912, USA
(Received 19 November 2009; revised manuscript received 9 February 2010; published 4 May 2010)

We report on ordering transitions of concentrated non-Brownian suspensions confined by two parallel walls under steady shear. At a volume fraction as low as $\phi=0.48$, particles near the wall assemble into strings which are organized as a simple hexagonal array by hydrodynamic interactions. The suspension exhibits a complex phase behavior depending on the ratio of the channel height to the particle radius, H_y/a. In a strongly confined system $H_y/a<12$, the order state and rheology depend on the commensurability between particle layers and the channel height. At $\phi=0.60$, the order structure in the horizontal plane changes between hexagonal and rectangular structures depending on H_y/a. It is shown that the relative viscosity is a function of both the volume fraction and the ordered state.

DOI: 10.1103/PhysRevE.81.051502 PACS number(s): 83.10.Tv, 47.57.E−, 47.15.G−, 83.50.Ha

I. INTRODUCTION

Colloidal suspensions undergo an intriguing phase behavior when subjected to a shear flow. In the absence of flow, a colloidal suspension develops a crystalline structure above a freezing volume fraction, $\phi_f=0.494$ for hard-sphere colloids [1,2], which can be melted by applying a strong shear to the system [3]. On the other hand, if a shear is applied to disordered colloidal suspensions for the volume fraction $\phi>\phi_f$, crystallization takes place rapidly at low shear rate yet it melts into a fluid at higher shear rate [4]. The shear melting is observed when the Péclet number $\mathrm{Pe}=6\pi\mu\dot{\gamma}a^3/k_BT$ is of $O(1)$. Here, μ is the viscosity of the solvent, $\dot{\gamma}$ is the shear rate, a is the particle radius, and k_BT is the thermal energy. Interestingly, another disorder-order transition has been observed at much higher shear rate $\mathrm{Pe}\gg1$ [5]. Sierou and Brady [6] have demonstrated the existence of shear-induced ordering in homogeneous non-Brownian suspensions ($\mathrm{Pe}\rightarrow\infty$) using the accelerated Stokesian dynamics simulations. Subsequently, Kulkarni and Morris [7] performed numerical simulations for a wide range of Pe, $1\leq\mathrm{Pe}\leq10^4$, and showed the similar phase behavior for $\mathrm{Pe}\geq10^3$. Nonequilibrium phase transitions, in general, are of interest both in theoretical studies [8] and in engineering applications [9]. As the dynamics are determined by a balance between driving forces, the process can be controlled by altering external fields. For example, in colloidal suspensions under an oscillatory shear, different types of crystalline structure can be obtained by changing the frequency and magnitude of the oscillation [10].

When a concentrated suspension is confined by solid boundaries, the dynamics of the suspension becomes dramatically different from the bulk properties [11–13]. In the absence of flow (Pe=0), phase behaviors of confined molecular or colloidal systems have been extensively studied over the last two decades (see [14] for review). Courtemanche and Swol [15] showed that crystallization of hard-sphere (HS) fluid occurs at a smooth boundary earlier than in the bulk fluid, i.e., below liquid-crystal coexistence, which is later known as "wall-induced ordering." Schmidt and Löwen [16] calculated the phase diagram of HS fluids confined by two parallel walls for $2<H/a<4$, where H is the separation distance between walls and a denotes the particle radius. Varying H/a for a fixed volume fraction ϕ, they observed strong discontinuous phase transitions between different crystal structures, e.g., layered, buckled, and rhombic crystals. Recently, Fortini and Dijkstra [17] performed extensive Monte Carlo simulations and calculated the equilibrium phase diagram of HS fluids for $2<H/a<10$. However, considering the relevance of highly confined suspensions to many industrial processes such as surface coating, lubricants, and microfluidic devices [18], surprisingly little is known for the effects of confinement on the dynamics of concentrated suspensions under shear flow. Sheared suspensions are different from the aforementioned equilibrium HS fluids in that the dynamics are determined by both long-range multibody hydrodynamic interactions and short-range lubrication and interparticle forces. In colloidal suspensions under oscillatory shear flows, Haw *et al.* [19] observed that crystal structures near a wall are more ordered than those in the center. However, they did not show any quantitative results. Cohen *et al.* [20] found that a new crystalline structure emerges in a strongly confined system in colloidal suspensions for $\phi=0.61\pm0.02$ under large oscillatory shear.

In this study, we report on the ordering transition of concentrated suspensions confined by two parallel walls under steady shear in the limit of infinite Pe, where dynamics are solely determined by hydrodynamic interactions and short-range interparticle forces. The particles near the walls start forming hexagonally organized strings in the plane normal to the flow at a volume fraction as low as $\phi\simeq0.48$, while the center of the channel remains disordered. The ordered state depends not only on the volume fraction but also on the ratio of the channel height to the particle radius H_y/a. The effect of the channel height on the order structure is investigated for $8\leq H_y/a\leq21$ at $\phi=0.52$.

In Sec. II, a brief review of the numerical method is presented. The main results of the numerical simulations are shown in Sec. III. Finally, the conclusions are given in Sec. IV.

*maxey@dam.brown.edu

II. NUMERICAL METHOD

The particle-particle and particle-wall hydrodynamic interactions are computed by the force-coupling method (FCM) together with lubrication corrections [21,22]. In FCM, far-field multibody interactions are calculated by solving the Stokes equations with a truncated, regularized multipole expansions. Near-field lubrication interactions are accounted for by inverting a resistance matrix constructed from the sum of particle-pair resistance matrices. FCM has been successfully employed for the numerical simulations of various suspension flows [13,23].

The equations of fluid motion with FCM for Stokes flows are

$$\frac{\partial p}{\partial x_i} = \mu \nabla^2 u_i + \sum_{n=1}^{N_p} \left\{ F_i^n \Delta_M(\boldsymbol{x} - \boldsymbol{Y}^n) + G_{ij}^n \frac{\partial}{\partial x_j} \Delta_D(\boldsymbol{x} - \boldsymbol{Y}^n) \right\}, \tag{1}$$

$$\boldsymbol{\nabla} \cdot \boldsymbol{u} = 0. \tag{2}$$

Here, p is pressure, μ is viscosity of fluid, $\boldsymbol{u}$ is fluid velocity, $\boldsymbol{Y}^n$ is the location of a particle center, and F_i and G_{ij} are the force monopole and force dipole moments, respectively. The FCM force envelopes Δ_M and Δ_D are given by

$$\Delta_M(\boldsymbol{x}) = \frac{1}{(2\pi\sigma_M^2)^{3/2}} \exp\left(-\frac{\boldsymbol{x}^2}{2\sigma_M^2} \right), \tag{3}$$

$$\Delta_D(\boldsymbol{x}) = \frac{1}{(2\pi\sigma_D^2)^{3/2}} \exp\left(-\frac{\boldsymbol{x}^2}{2\sigma_D^2} \right), \tag{4}$$

in which $\sigma_M = a/\sqrt{\pi}$ and $\sigma_D = a/(6\sqrt{\pi})^{1/3}$. The force monopole and dipole moments are

$$F_i = F_i^P - F_i^{lub}, \tag{5}$$

$$G_{ij} = S_{ij}^{FCM} - T_{ij}^{lub}. \tag{6}$$

Here, $\boldsymbol{F}^P$ is an external force on the particles and $\boldsymbol{F}^{lub}$ and $\boldsymbol{T}^{lub}$ are the Stokeslet and couplet coefficients for the lubrication corrections, respectively. The FCM stresslet $\boldsymbol{S}^{FCM}$ is related with the particle stresslet $\boldsymbol{S}$ as

$$\boldsymbol{S}^{FCM} = \boldsymbol{S} + \boldsymbol{R}_{ES}\boldsymbol{E}^\infty - [\boldsymbol{R}_{VS}(\boldsymbol{V} - \boldsymbol{V}^\infty) + \boldsymbol{R}_{\Omega S}(\boldsymbol{\Omega} - \boldsymbol{\Omega}^\infty)], \tag{7}$$

in which $\boldsymbol{R}_{AB}$ is a resistance matrix relating A to B, and $\boldsymbol{V}$ and $\boldsymbol{\Omega}$ are, respectively, vectors for the translational and angular velocities of the particles. The resistance matrix is constructed in a pairwise manner from the exact two-body resistance matrix, subtracting the FCM two-body resistance matrix, to account for the lubrication forces. $\boldsymbol{V}^\infty$, $\boldsymbol{\Omega}^\infty$, and $\boldsymbol{E}^\infty$ are $\boldsymbol{V}$, $\boldsymbol{\Omega}$, and a vector for the strain rate of the imposed Couette flow, respectively. Once $\boldsymbol{u}$ is computed by solving the governing equations, $\boldsymbol{V}$ and $\boldsymbol{\Omega}$ are obtained by

$$\boldsymbol{V}^n = \int \boldsymbol{u}(x) \Delta_M(\boldsymbol{x} - \boldsymbol{Y}^n) d^3\boldsymbol{x}, \tag{8}$$

$$\Omega_i^n = \frac{1}{2} \int \epsilon_{ijk} \frac{\partial u_k}{\partial x_j} \Delta_D(\boldsymbol{x} - \boldsymbol{Y}^n) d^3\boldsymbol{x}. \tag{9}$$

Note that, since $\boldsymbol{F}^{lub}$, $\boldsymbol{\Omega}^{lub}$, and $\boldsymbol{S}^{FCM}$ are functions of both $\boldsymbol{V}$ and $\boldsymbol{\Omega}$, an iterative procedure is necessary to solve the system. An efficient iterative scheme is given in Yeo and Maxey [22].

Now, it is well known that short-range nonhydrodynamic interactions between particles are responsible for the non-Newtonian rheology of concentrated suspensions [24]. The nonhydrodynamic effects may come from roughness elements on particle surface, residual Brownian forces, surface charge, to name a few. For example, typically noncolloidal particles [$a \geq O(10\ \mu\text{m})$] have roughness elements on the order of $10^{-2}a - 10^{-3}a$ [25] and the repulsive potential of sterically stabilized colloids is softer than that of hard spheres, which can be modeled as a hard core with a soft tail potential [2,26]. To model these nonhydrodynamic effects, we employ a contact force model. The contact force on particle i from particle j is given by

$$\boldsymbol{F}_C^{ij} = \begin{cases} -6\pi\mu\dot{\gamma}a^2 F_{ref} \left(\dfrac{R_{ref}^2 - |\boldsymbol{r}|^2}{R_{ref}^2 - 4a^2} \right)^6 \dfrac{\boldsymbol{r}}{|\boldsymbol{r}|} & \text{if } |\boldsymbol{r}| < R_{ref} \\ 0 & \text{otherwise,} \end{cases} \tag{10}$$

in which $\boldsymbol{r} = \boldsymbol{Y}^i - \boldsymbol{Y}^j$, F_{ref} is a constant, and R_{ref} is a cut-off distance. In the present study, the contact force is activated if the shortest distance between two particle surfaces (ϵ) is less than $0.01a$, i.e., $R_{ref}/a = 2.01$. F_{ref} is chosen to keep the minimum separation distance $\epsilon_{\min} \simeq 0.002a$. $F_{ref} = 200$ is used for $\phi = 0.46 - 0.54$ and $F_{ref} = 600$ for $\phi = 0.60$. Once $\boldsymbol{F}_C$ is computed for all the neighboring particles, it is added to $\boldsymbol{F}^P$.

Equations (1) and (2) are solved by using a Fourier spectral method in the velocity (x) and the vorticity (z) directions and a spectral element method in the velocity-gradient direction (y) [27]. The computational domain in x and z directions are fixed, $H_x/a = 30$ and $H_z/a = 20$, and H_y is varied; $8 \leq H_y/a \leq 30$. Periodic boundary conditions are used in x and z directions. The number of particles ranges from 688 for $\phi = 0.48$ and $H_y/a = 10$ to 2 235 for $\phi = 0.52$ and $H_y/a = 30$.

To generate initial configurations, small particles are seeded randomly in the computational domain. Then, a molecular dynamics simulation with a repulsive potential is performed, while slowly increasing the particle radius until the desired volume fraction is reached. Figure 1 shows the development of the relative viscosity μ_r in time for $H_y/a = 20$. Once shear is applied, the suspension exhibits a disordered fluid state at first [Fig. 1(b)], which accompanies a sharp increase in μ_r. The peak μ_r is observed to be in between the high-frequency shear viscosity and the dynamic shear viscosity. For $\phi = 0.60$, the peak μ_r is around 70. As order develops [Fig. 1(c)], μ_r drops slowly. In most cases, a stationary state is reached after $\dot{\gamma}t \simeq 40 - 50$, which is much faster than for the homogeneous shear results in Kulkarni and Morris [7] ($\dot{\gamma}t \simeq 150$).

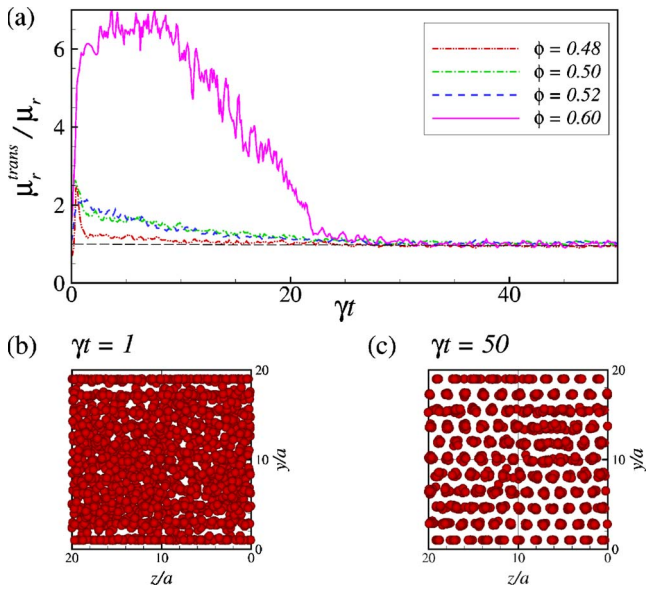

FIG. 1. (Color online) (a) Transient behavior of the relative viscosity normalized by the relative viscosity in the stationary state. The channel height is fixed; $H_y/a=20$. Snapshots (end view) for $\phi=0.52$ and $H_y/a=20$ at $\dot{\gamma}t=1$ (b) and 50 (c). For visualization, the particle radius is reduced to 1/2 of the actual size.

III. RESULTS

In wall-bounded suspensions, the behavior of suspensions near the wall is radically different from the center of the channel. Depending on the microstructures, Yeo and Maxey [13] showed that the wall-bounded suspensions of non-Brownian particles can be divided into three regions, the wall, buffer, and core regions. The wall region is distinguished by a strong particle layering. In the core region, the suspension is similar to that in a homogeneous shear flow. In the buffer region, the suspension microstructure is no longer reflexional symmetric due to the interactions with particle layers below (wall region) and the shear structure above (core region). To show the different levels of ordering near the wall and in the channel center, we investigate the microstructures in the wall Ω^W and the core Ω^C regions; $\Omega^W=(0,H_x)\times\{(0,1.5a)\cup(H_y-1.5a,H_y)\}\times(0,H_z)$ and $\Omega^C=(0,H_x)\times(5a,H_y-5a)\times(0,H_z)$. For $H_y/a=10$, Ω^C is defined as $\Omega^C=(0,H_x)\times(4a,6a)\times(0,H_z)$.

First, the ordering transition is investigated by varying ϕ for $H_y/a=20$. The pair distribution function in spherical polar coordinates $g(r,\theta,\psi)$ is calculated for particles in Ω^W and Ω^C, in which r is the radial distance, θ is the azimuthal angle measured from the velocity direction, and ψ denotes the polar angle measured from the vorticity direction. Figure 2 shows $g(r,\theta,\psi)$ in the velocity gradient—vorticity $(y-z)$ plane, i.e., $\theta=\pi/2$. At $\phi=0.46$, the dominant structure in Ω^W is the particle layering and a weak hexagonal order is observed, while $g(r,\psi)$ in Ω^C shows an isotropic ringlike structure indicating the suspension is homogeneous. At $\phi=0.48$, a hexagonal order begins to be developed in Ω^W, while the suspension in Ω^C is still in disordered state. At $\phi=0.52$, the whole channel is almost completely ordered [Fig. 2(c)]. As the suspension in Ω^C is in the disorder-order coexistence state, $g(r,\psi)$ for $\phi=0.50$ shows a mixture of the hexagonal structure [Fig. 2(d)] and the ringlike structure [Fig. 2(c)].

Figure 3 shows the area fraction ϕ_A as a function of y for $H_y/a=20$. ϕ_A is calculated by $\phi_A=\int\int\chi(\boldsymbol{x})dxdz/(H_x\times H_z)$. Here, $\chi(\boldsymbol{x})$ is an indicator function which is nonzero if $\boldsymbol{x}$ is inside of particles. For $\phi\leq 0.46$, ϕ_A is higher near the wall. The values of the first peaks near the walls are insensitive to ϕ. It seems that the high volume fraction near the wall leads to the earlier transition in Ω^W than in Ω^C. At $\phi=0.46$, the value of the local peaks is a decreasing function of distance

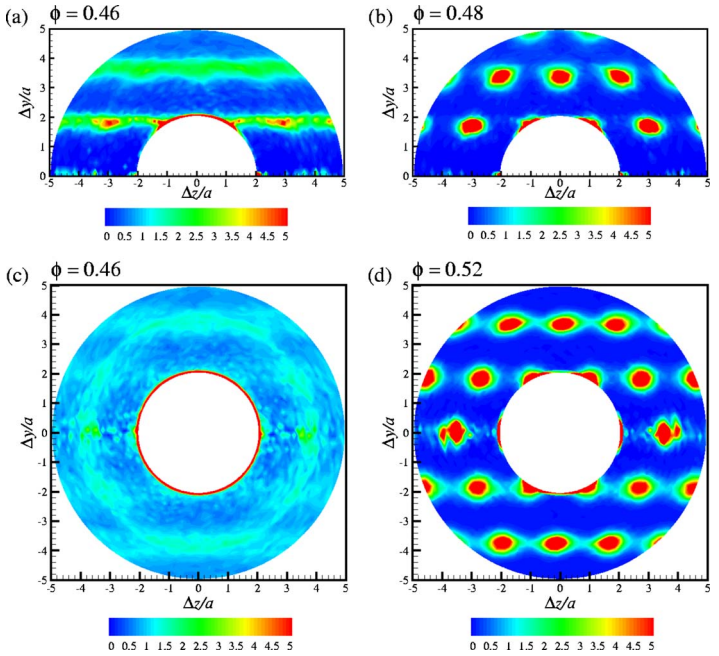

FIG. 2. (Color online) Two-dimensional pair distributions in the velocity-gradient-vorticity $(y-z)$ plane for $H_y/a=20$ obtained in (a) and (b) Ω^W and (c) and (d) Ω^C.

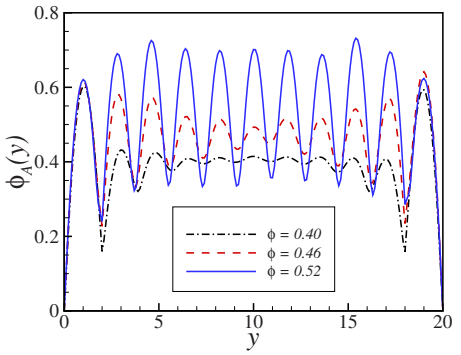

FIG. 3. (Color online) Area fraction profiles for $H_y/a=20$.

from the wall. Similar to $\phi=0.40$, if H_y/a is large enough, ϕ_A may become uniform around the core of the channel. However, once the ordered structure is present across the entire channel ($\phi=0.52$), ϕ_A is no longer a decreasing function of distance from the wall. The peaks of ϕ_A are almost constant across the channel. The area fraction profiles suggest that the particles form a layered structure at high volume fractions in confined suspensions, in which the suspension dynamics are dependent on the interaction between discrete particle layers, and, thus, the previous continuum model approaches, which rely on the rheological functions based on well-mixed suspensions, may not be suitable to apply for suspensions near the ordering transitions.

Figure 4 shows the hexagonal order parameter C_6 estimated in Ω^W and Ω^C. Similar to the bond-orientational order parameter, C_6 is defined as [7]

$$C_6 = \frac{\int_0^{2\pi} g(\psi)\cos(6\psi)d\psi}{\int_0^{2\pi} g(\psi)d\psi}, \tag{11}$$

in which $g(\psi)$ is the pair-distribution function in the $y-z$ plane averaged over $2a<r<2.1a$. The values of C_6 lie in the range $0\leq C_6\leq 1$, i.e., $C_6=1$ for a perfect hexagonal structure and $C_6=0$ for an isotropic microstructure. In general, C_6 in Ω^W is larger than that in Ω^C consistent with the wall-induced ordering. For $H_y/a=15$, the hexagonal ordering in Ω^W is not evident when $\phi\leq 0.48$. On the other hand, for $H_y/a=20$, $C_6\simeq 0.8$ at $\phi=0.48$, indicating that the particles in Ω^W begin to be ordered into hexagonal strings at $\phi=0.48$. When $\phi\geq 0.52$ and $H_y/a=20$, C_6 in Ω^C and Ω^W are almost the same, implying the presence of the hexagonal order in the whole channel. The decrease in C_6 in Ω^W at high volume fraction is

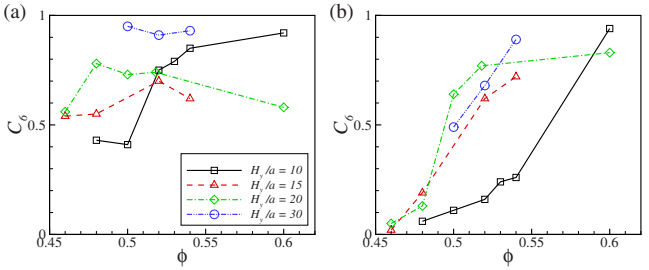

FIG. 4. (Color online) Order parameter C_6 in (a) Ω^W and (b) Ω^C.

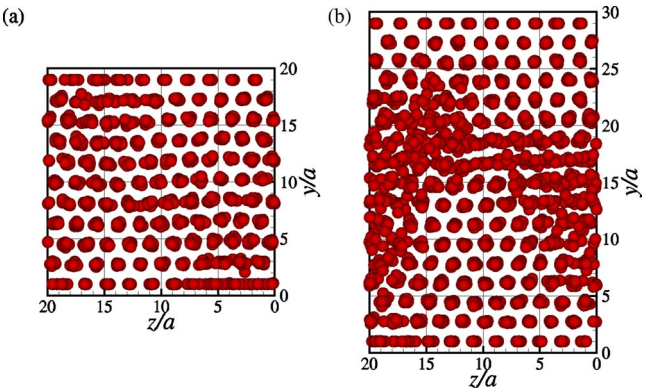

FIG. 5. (Color online) Snapshots (end view) for $\phi=0.52$; (a) $H_y/a=20$ and (b) $H_y/a=30$. For visualization, the particle radius is reduced to 1/2 of the actual size.

mainly due to the small sampling volume. Since the sampling volume of C_6 for Ω^W is small, even if there are only a few defects in the sampling volume, C_6 can be significantly reduced by these defects. If C_6 is computed for the whole domain, it is a nondecreasing function of ϕ for a given H_y/a.

In a larger channel ($H_y/a=30$), the wall effects become weaker in the channel center, which in turn weakens the ordered structure in Ω^C. At $\phi=0.50$, C_6 in Ω^C are 0.65 and 0.5 for $H_y/a=20$ and 30, respectively. On the other hand, a better order is observed near a wall. Figure 5 shows snapshots for different H_y at $\phi=0.52$. For $H_y/a=20$, most particles are assembled into nearly linear strings which are organized as a hexagonal array with a few defects. However, for $H_y/a=30$, a disordered fluid region emerges in the channel core. Typically, most experiments of noncolloidal suspensions are performed in a wide channel, for example $H_y/a>40$ [28]. Therefore, it is likely that the suspension is in the disorder-order coexistence state, for which the bulk behavior resembles that of the homogeneous suspension. This may be one reason that ordering transitions in the noncolloidal suspension has not been investigated so far in experiments.

The relative viscosity μ_r is shown in Fig. 6. For $H_y/a=15$ and 20, μ_r begins to decrease at $\phi=0.48$ as the hexagonal order develops. Once the hexagonal order is dominant across the entire channel, μ_r increases again ($\phi>0.52$). The value of μ_r for $H_y/a=30$ is larger than those in the smaller

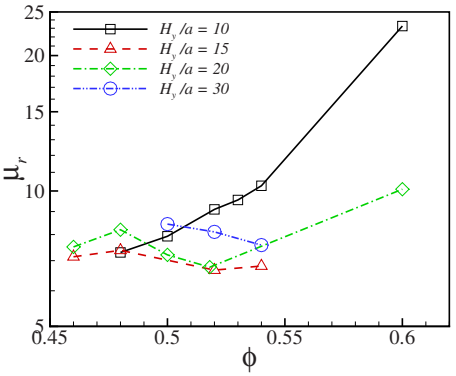

FIG. 6. (Color online) The relative viscosity for various ϕ and H_y/a.

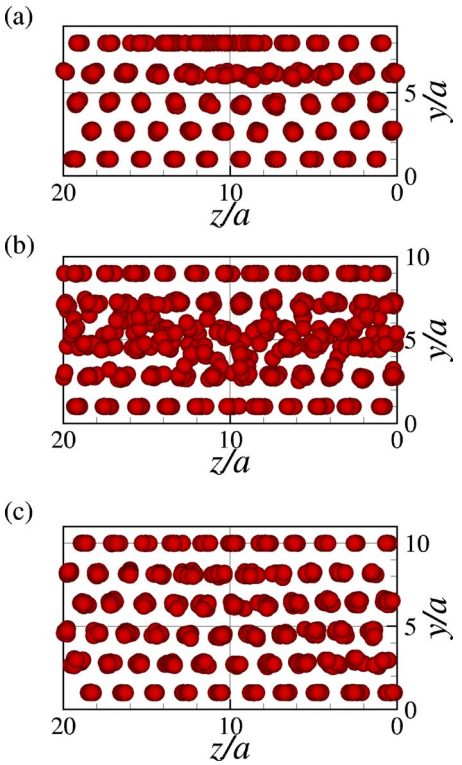

FIG. 7. (Color online) Snapshots (end view) for ϕ=0.52; (a) H_y/a=9, (b) H_y/a=10, and (c) H_y/a=11. For visualization, the particle radius is reduced to 1/2 of the actual size.

channels due to the emergence of disordered region in Ω^C, in which μ_r is higher. It is expected that, in a large channel $H_y/a>40$, the disordered region is much larger than the ordered region so that the bulk properties would resemble those without the ordered structures. Unlike the results in the three wider channels, μ_r for H_y/a=10 is an increasing function of ϕ.

In the equilibrium phase transition (Pe=0) of strongly confined colloidal suspensions, a sequence of crystal layers is observed depending on the commensurability of the crystal structures with the channel height; $n\square \rightarrow n\triangle \rightarrow (n+1)\square \rightarrow \cdots$ Here, $n\square$ and $n\triangle$, respectively, denote n crystal layers of square and hexagonal lattice symmetries in the horizontal $(x-z)$ plane. Depending on the commensurability, first-order melting and freezing transitions are observed between different crystal structures [16]. At higher volume fractions, the alternating sequence of square and hexagonal crystal layers is disturbed by the emergence of other crystal structures such as rhombic, buckling, or prism phases [17]. In flowing suspensions, the particle layers slide over each other and ordered structures must accommodate this. Hence, it is not expected that the ordered structures and the commensurability

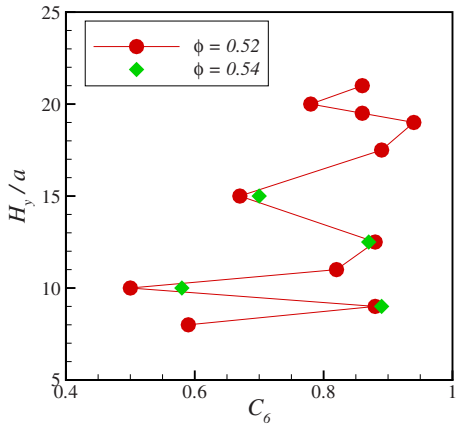

FIG. 8. (Color online) The order parameter as a function of H_y/a for ϕ=0.52 and 0.54.

will exactly follow what has been observed in the thermodynamic phase transitions of HS fluids or colloidal suspensions.

To investigate the effects of H_y/a on the ordering transition in flowing suspensions, the numerical simulations are performed for varying H_y/a from 8 to 20 for ϕ=0.52 and 0.54. Figure 7 shows snapshots for ϕ=0.52 at different channel heights H_y/a. Increasing H_y/a from 9 to 11, it is shown that the suspension exhibits phase transitions from the hexagonal order [Fig. 7(a)] to a mixed state [Fig. 7(b)] and, then, again to the ordered state [Fig. 7(c)].

Figure 8 shows the order parameter C_6 as a function of H_y/a for ϕ=0.52 and 0.54. It is shown that the order structure is very sensitive to H_y when $H_y/a \leq 11$. For ϕ=0.52, the suspensions are in an ordered state for H_y/a=9 and 11 and in a disordered state for H_y/a=8 and 10. The similar behavior is observed for ϕ=0.54. The oscillation in C_6 becomes smaller for larger H_y. When H_y/a is changed from 10 to 11, C_6 decreases from 0.88 to 0.50, while, increasing H_y/a=19 to 20, it changes from 0.94 to 0.78.

The change in the order state is due to the commensurability of the order structures with the available space between two walls. As the most distinguishable structure is the simple hexagonal lattice in the $y-z$ plane, a characteristic gap width can be defined as

$$\eta = \frac{H_y - 2a}{\sqrt{3}a} + 1. \tag{12}$$

The characteristics gap width are shown in Table I together with the number of particle layers N and the order parameter C_6. The number of particle layer is well approximated by η. As expected, the suspension is in more ordered state (large C_6) when η is close to an integer, or small $|N-\eta|$. When η is increased or decreased from an integer, the distance between

TABLE I. Channel height H_y/a, characteristic gap width η, number of particle layers N, and order parameter C_6 for ϕ=0.52.

H_y/a	8	9	10	11	12.5	15	17.5	19	19.5	20	21
η	4.46	5.04	5.62	6.20	7.06	8.51	9.95	10.82	11.10	11.39	11.97
N		5		6	7	8	10	11	11	11	12
C_6	0.59	0.88	0.50	0.82	0.88	0.67	0.89	0.94	0.86	0.78	0.86

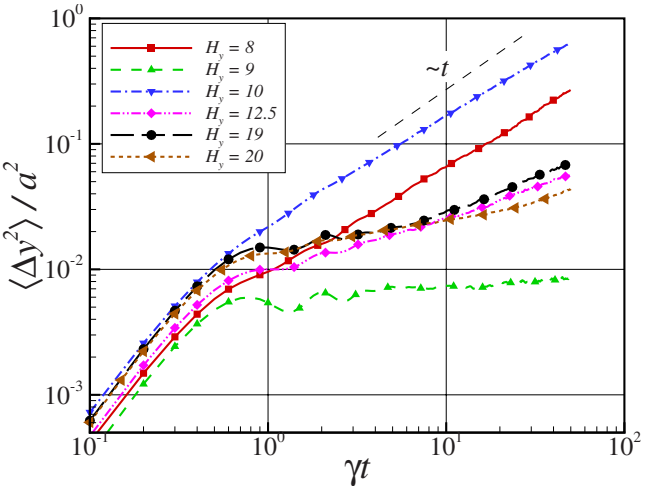

FIG. 9. (Color online) The normalized mean-square vertical displacements $\langle [Y_2(t) - Y_2(0)]^2 \rangle / a^2$ for $\phi = 0.52$.

particle layers increases making particles more mobile. As a result, the order structure becomes unstable and the suspension becomes disordered.

The mean-square displacement (MSD) in the vertical direction $\langle [Y_2(t) - Y_2(0)]^2 \rangle$ normalized by a^2 is shown in Fig. 9. After a short ballistic regime ($\dot{\gamma} t \sim O(10^{-1})$), MSDs for $H_y/a = 8$ and 10 show a subdiffusive behavior, $\langle [Y_2(t) - Y_2(0)]^2 \rangle \sim t^{\nu}$ with the exponent $\nu = 0.86$ on the intermediate time scale of the present simulation. Yeo and Maxey [29] showed that confined non-Brownian suspensions for $\phi = 0.40$ exhibit subdiffusion on the time scale of $\dot{\gamma} t \sim O(100)$. In the long term, the vertical particle displacement is confined by the size of the channel height. When an ordered structure is developed, the vertical displacement of particles is restricted by the cage formed by neighboring particles. For $H_y/a = 19$ and 20, in which the suspensions are in a mixed state, the particles in the core of the channel behaves similarly to the disordered state, while mobility of the particles near the walls is significantly reduced due to the ordered structure. Hence, MSDs for $H_y/a = 19$ and 20 are significantly lower than those in a disordered state ($H_y/a = 8$ and 10). For $H_y/a = 9$, the entire channel is in an ordered state and the vertical displacement of particles is observed only near defects. Hence, there is a large increase in MSDs between ordered ($H_y/a = 9$) and mixed states ($H_y/a = 12.5$, 19, and 20).

The bulk particle pressure Π normalized by $\mu \dot{\gamma}$ is shown in Fig. 10. The definition of Π is

$$\Pi = -\frac{1}{3}(\sigma_{11} + \sigma_{22} + \sigma_{33}). \tag{13}$$

Here, σ_{ij} denotes the particle stress computed from the stresslet and the interparticle potential. In a strongly confined system ($H_y/a < 12$), the oscillation of Π is almost exactly opposite to C_6. However, in larger channels, the correlation between Π and C_6 becomes less clear. Because the wall effect is strong across the entire channel in small channels, the order structure and, thus, the rheological parameters are mainly determined by the commensurability. On the other hand, in a larger channel, there is a competition between the confinement effect and the shear-induced hydrodynamic interactions around the core of the channel. Therefore, rheology does not exactly follow the commensurability of the channel.

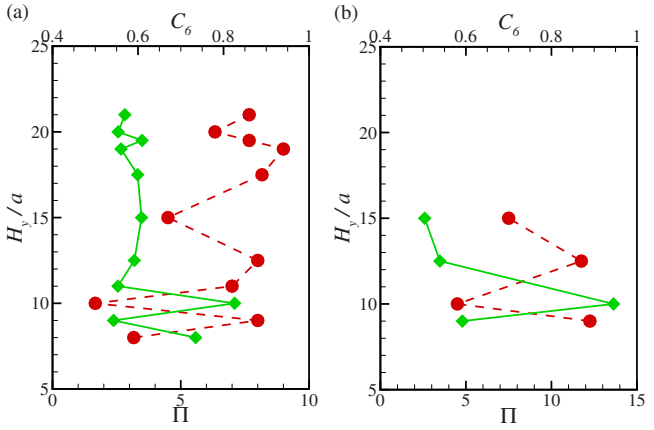

FIG. 10. (Color online) The particle pressure Π (♦) and the order parameter C_6 (●) as a function of H_y/a for (a) $\phi = 0.52$ and (b) 0.54.

Figure 11(a) shows the order structure in the horizontal ($x-z$) plane for $\phi = 0.52$ and $H_y/a = 9$. A rhombic phase is observed for the horizontal structure. A stable rhombic phase is also observed in the equilibrium phase transitions of con-

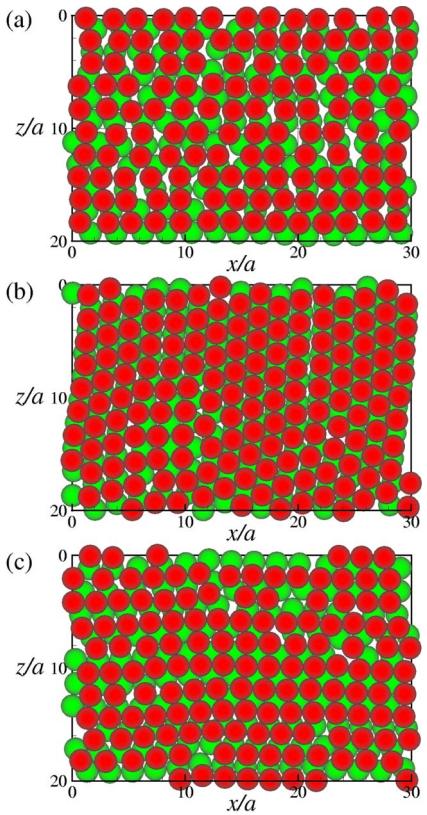

FIG. 11. (Color online) Order structures in the horizontal plane for (a) $\phi = 0.52$ and $H_y/a = 9$, (b) $\phi = 0.60$ and $H_y/a = 9$, and (c) $\phi = 0.60$ and $H_y/a = 10$. Green (lighter) particles are in the lower layer and red (darker) particles are in the upper layer.

fined HS fluids as an interpolating structure between square and hexagonal symmetric structures [16]. Fortini and Dijkstra [17] found that the rhombic phase is stable between $n\square$ and $n\triangle$ for $n \leq 5$, i.e., $H_y/a < 10$. However, in flowing suspensions, a rhombic phase is observed for a wide range of H_y/a. When $\phi \leq 0.54$, only rhombic phases are observed for the range of parameters in the present study of non-Brownian (infinite Pe) suspensions. In flowing suspensions, the disturbance flow induced by a particle decays slowly, which leads to a long-range correlation. The long-range hydrodynamic interactions result in the earlier order transition in sheared non-Brownian suspensions than that seen in HS fluids. However, near the lower boundary of order transitions, the volume fraction is still too low to develop a fully three-dimensional crystal structure. As the hydrodynamic force induced by the shear flow is anisotropic, an ordered structure is formed in the $y-z$ plane first. It seems that the rhombic phase in the $x-z$ plane in Fig. 11(a) is a transitional structure that supports a hexagonal structure in the $y-z$ plane at the given volume fraction. In contrast, suspensions at higher volume fractions may show a phase behavior similar to HS fluids. At $\phi=0.60$, 5 layers of the hexagonal symmetric structure are observed for $H_y/a=9$ [Fig. 11(b)], which is followed by 6 layers of nearly rectangular structure for $H_y/a=10$ [Fig. 11(c)].

IV. CONCLUSIONS

We have made a first investigation of ordering transitions of non-Brownian suspensions confined by two parallel walls under steady shear. We show that the shear-induced crystallization of non-Brownian suspensions under a strong confinement is dramatically different from the previous results in homogeneous suspensions. As the volume fraction is higher near the wall than the bulk, an ordering transition occurs earlier in the wall region. At $\phi=0.48$ and $H_y/a \geq 15$, a hexagonal structure ($y-z$ plane) of particle strings (x direction) is observed near the wall, while the suspension in the core of the channel is still in disordered state. For a strongly confined system $H_y/a \leq 11$, the order state and rheology depend on the commensurability. However, due to the competition between the wall effects and shear-induced hydrodynamic forces, the relation is not so clear for larger channels $H_y/a \geq 20$. At $\phi=0.60$, it is observed that the order structure in horizontal plane exhibits a transition from triangular to rectangular structures, similar to the equilibrium phase transitions in HS fluids. It is shown that due to the complex phase behavior, the rheological parameters, such as the relative viscosity and the particle pressure, are nonlinear functions of both the channel height and the volume fraction.

ACKNOWLEDGMENTS

We thank the anonymous referees and Professor J. F. Morris of City College, New York for their helpful comments. This research was supported in part by the National Science Foundation under Grant No. DUE-0734234 and an allocation of advanced computing resources provided by the National Science Foundation under Grant No. TG-CTS090097. The computations were performed on Kraken (a Cray XT5) at the National Institute for Computational Sciences (http://www.nics.tennessee.edu/).

[1] P. N. Pusey and W. van Megen, Nature (London) **320**, 340 (1986).
[2] W. B. Russel, D. A. Saville, and W. R. Schowalter, *Colloidal Dispersions* (Cambridge University Press, Cambridge, 1989).
[3] D. Derks, Y. Wu, A. van Blaaderen, and A. Imhof, Soft Matter **5**, 1060 (2009).
[4] Y. Wu, D. Derks, A. van Blaaderen, and A. Imhof, Proc. Natl. Acad. Sci. U.S.A. **106**, 10564 (2009).
[5] B. J. Ackerson, J. Rheol. **34**, 553 (1990).
[6] A. Sierou and J. F. Brady, J. Rheol. **46**, 1031 (2002).
[7] S. D. Kulkarni and J. F. Morris, J. Rheol. **53**, 417 (2009).
[8] L. Corté, P. M. Chaikin, J. P. Gollub, and D. J. Pine, Nat. Phys. **4**, 420 (2008); L. Corté, S. J. Gerbode, W. Man, and D. J. Pine, Phys. Rev. Lett. **103**, 248301 (2009).
[9] M. Fialkowski, K. J. M. Bishop, R. Klajn, S. K. Smoukov, C. J. Campbell, and B. A. Grzybowski, J. Phys. Chem. B **110**, 2482 (2006).
[10] J. M. McMullan and N. J. Wagner, J. Rheol. **53**, 575 (2009).
[11] C. R. Nugent, K. V. Edmond, H. N. Patel, and E. R. Weeks, Phys. Rev. Lett. **99**, 025702 (2007); V. N. Michailidou, G. Petekidis, J. W. Swan, and J. F. Brady, *ibid.* **102**, 068302 (2009).
[12] H. B. Eral, D. van den Ende, F. Mugele, and M. H. G. Duits, Phys. Rev. E **80**, 061403 (2009).
[13] K. Yeo and M. R. Maxey, J. Fluid Mech. **649**, 205 (2010).
[14] S. A. Rice, Chem. Phys. Lett. **479**, 1 (2009).
[15] D. J. Courtemanche and F. van Swol, Phys. Rev. Lett. **69**, 2078 (1992).
[16] M. Schmidt and H. Löwen, Phys. Rev. Lett. **76**, 4552 (1996); Phys. Rev. E **55**, 7228 (1997).
[17] A. Fortini and M. Dijkstra, J. Phys.: Condens. Matter **18**, L371 (2006).
[18] D. J. Shaw *Introduction to Colloid and Surface Chemistry* (Butterworths, Boston, 1980); S. Granick, Phys. Today **52** 7, 26 (1999); D. Psaltis, S. R. Quake, and C. Yang, Nature (London) **442**, 381 (2006).
[19] M. D. Haw, W. C. K. Poon, and P. N. Pusey, Phys. Rev. E **57**, 6859 (1998).
[20] I. Cohen, T. G. Mason, and D. A. Weitz, Phys. Rev. Lett. **93**, 046001 (2004).
[21] S. Lomholt and M. R. Maxey, J. Comput. Phys. **184**, 381 (2003).
[22] K. Yeo and M. R. Maxey, J. Comput. Phys. **229**, 2401 (2010).
[23] E. Climent, M. R. Maxey, and G. E. Karniadakis, Langmuir **20**, 507 (2004); M. Abbas, E. Climent, O. Simonin, and M. R. Maxey, Phys. Fluids **18**, 121504 (2006); E. E. Keaveny and M. R. Maxey, Phys. Rev. E **77**, 041910 (2008).
[24] J. F. Brady and J. F. Morris, J. Fluid Mech. **348**, 103 (1997).

[25] J. R. Smart and D. T. Leighton, Phys. Fluids A **1**, 52 (1989).
[26] U. Genz, B. D'Aguanno, J. Mewis, and R. Klein, Langmuir **10**, 2206 (1994).
[27] S. L. Dance and M. R. Maxey, Phys. Rev. E **68**, 031403 (2003).
[28] I. E. Zarraga, D. A. Hill, and D. T. Leighton, J. Rheol. **44**, 185 (2000).
[29] K. Yeo and M. R. Maxey (unpublished).